

Tunable anisotropic superfluidity in an optical kagome superlattice

Xue-Feng Zhang (张学锋)^{1,2} Tao Wang (汪涛)^{1,3} Sebastian Eggert,¹ and Axel Pelster^{1,*}

¹Physics Department and Research Center OPTIMAS, Technical University of Kaiserslautern, 67663 Kaiserslautern, Germany

²State Key Laboratory of Theoretical Physics, ITP, Chinese Academy of Sciences, Beijing 100190, China

³Department of Physics, Harbin Institute of Technology, Harbin 150001, China

(Received 5 May 2015; revised manuscript received 2 July 2015; published 27 July 2015)

We study the phase diagram of the Bose-Hubbard model on the kagome lattice with a broken sublattice symmetry. Such a superlattice structure can naturally be created and tuned by changing the potential offset of one sublattice in the optical generation of the frustrated lattice. The superstructure gives rise to a rich quantum phase diagram, which is analyzed by combining quantum Monte Carlo simulations with the generalized effective potential Landau theory. Mott phases with noninteger filling and a characteristic order along stripes are found, which show a transition to a superfluid phase with an *anisotropic* superfluid density. Surprisingly, the direction of the superfluid anisotropy can be tuned by changing the particle number, the hopping strength, or the interaction. Finally, we discuss characteristic signatures of anisotropic phases in time-of-flight absorption measurements.

DOI: [10.1103/PhysRevB.92.014512](https://doi.org/10.1103/PhysRevB.92.014512)

PACS number(s): 67.85.-d, 05.30.Jp, 75.40.Mg, 78.67.Pt

I. INTRODUCTION

Ultracold atoms in optical lattices are prominently used to simulate many-body systems in condensed-matter physics [1–5]. One of the most striking experiments is the Mott insulator–superfluid quantum phase transition of ultracold bosons in an optical lattice built with counterpropagating lasers [6]. It can be described by the seminal Bose-Hubbard model [7,8], where each parameter is precisely adjustable in the experiment. With the rapid advances in experimental techniques, many-body physics can now be analyzed on more complex lattice geometries [9]. On the one hand, the lattice symmetry can be reduced by adding additional lasers or tuning their relative strength, leading to a superlattice structure [10–13], which can give rise to insulator phases with fractional fillings [14–19]. On the other hand, it is also possible to *enhance* the residual entropy of the many-body system by using frustrated lattices, which have recently been realized using sophisticated optical techniques [20–22].

Theoretically, many interesting phases have been predicted in frustrated lattices such as spin liquids [23–29], valence bond solids [30], string excitations [31], ordered metals [32], chiral fractional edge states [33], and supersolids [34–37]. Unfortunately, in all these scenarios, longer range interactions beyond the on-site Bose-Hubbard model are assumed, which require dipolar interactions and are experimentally much harder to handle. However, the intriguing interplay between a superlattice and the kagome lattice can lead to fractional-filled Mott phases with a highly nontrivial phase diagram [15] without the need for longer range interactions. In this paper we now theoretically and numerically analyze a tunable kagome superlattice, which corresponds to a straightforward extension of a recently realized experimental setup [22]. As expected, we find fractionally filled ordered phases, which are surprisingly large and stable in the quantum phase diagram. The most interesting behavior occurs in the superfluid phase, which is characterized by an anisotropic superfluid density. Remarkably, the dominant superfluid direction is not fixed

by the superlattice, but instead becomes *tunable* as a function of filling, hopping, and interaction. The corresponding characteristic signatures in time-of-flight absorption pictures are discussed below. The behavior of the tunable anisotropy can be explained only by a certain amount of density-wave order, which is still present in regions of the superfluid phase. Even though the translation invariance is not spontaneously broken in this case, we will call these regions “supersolid-like,” since they enable the study of the interplay between density-wave order and superfluidity without the need for long-range interactions.

II. THE OPTICAL LATTICE

Let us first consider the optical generation of a kagome lattice, which recently has been achieved experimentally by using standing waves from a long-wavelength 1064-nm (LW) laser and from a short-wavelength 532-nm (SW) laser, which are counterpropagating from three 120° directions [22]. The superposition of the corresponding two triangular lattices results in a kagome lattice if the laser strengths are exactly equal from all directions. Any slight variation of this setup results in a superlattice structure, which of course can be used as an additional tunable parameter. For example, enhancing the potential from the LW laser in the x direction by the factor $\gamma = V_E/V_0 > 1$ results in the combined optical potential

$$V_c/V_0 = \gamma^2 - 1 + 4\gamma \cos(\sqrt{3}kx) \cos(ky) + 2 \cos(2ky) - 2 \cos(4ky) - 4 \cos(2\sqrt{3}kx) \cos(2ky), \quad (1)$$

where $k = \sqrt{3}\pi/2\lambda_{LW}$ in units of the longer wavelength $\lambda_{LW} = 1064$ nm. As depicted in Fig. 1 this potential leads to an offset of $\Delta\mu = 4(\gamma - 1)V_0 > 0$ on one of the sublattices A. Note, however, that this offset preserves the parity symmetry along the x and y directions and does not increase the unit cell of the kagome lattice, which contains three sites.

Interacting bosons on this lattice can be represented by Wannier states, which leads to the well-known Bose-Hubbard model for the description of the lowest band in second

*axel.pelster@physik.uni-kl.de

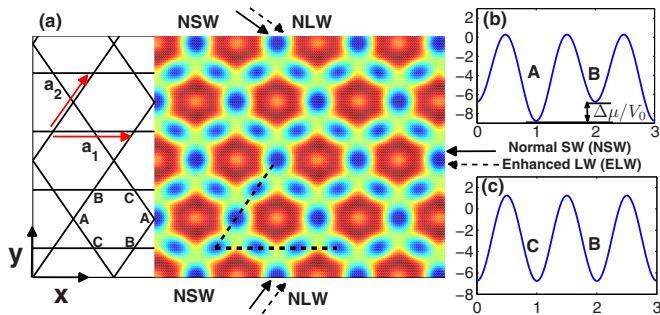


FIG. 1. (Color online) (a) Potential from Eq. (1) of the optical kagome superlattice using an enhanced LW laser in the x direction with $\gamma = 1.5$. Potential along cuts (dashed lines) in the (b) a_2 direction and (c) a_1 direction, respectively, showing the resulting potential offset $\Delta\mu$ for sublattice A.

quantized language

$$H = -t \sum_{\langle i,j \rangle} (\hat{a}_i^\dagger \hat{a}_j + \hat{a}_i \hat{a}_j^\dagger) + \frac{U}{2} \sum_i \hat{n}_i (\hat{n}_i - 1) - \mu \sum_i \hat{n}_i - \Delta\mu \sum_{i \in A} \hat{n}_i, \quad (2)$$

where the nearest-neighbor hopping amplitude t and the on-site interaction U are tunable parameters, which depend on the scattering cross section and the potential depth V_0 [4]. In principle, the potential shift $\Delta\mu$ also affects the Wannier states and hence other parameters in Eq. (2), but for reasonably small values of $\Delta\mu$ these higher order corrections can be neglected since they preserve the symmetry of the problem. The chemical potential μ is used to tune the particle number in the grand-canonical ensemble. In the following we will use the stochastic cluster series expansion algorithm [38–40] for unbiased quantum Monte Carlo (QMC) simulations of this model. In addition the generalized effective potential Landau theory (GEPLT) provides an analytic method to estimate the phase boundaries in an expansion of the hopping parameter t/U [19,41]. The method relies on systematically including quantum fluctuations in an effective potential for the Landau theory.

III. PHASE DIAGRAM

For vanishing hopping amplitude t in the atomic limit, the competition between U and $\Delta\mu$ can induce several incompressible insulating phases. When μ is less than $-\Delta\mu$, no site is occupied, and the Mott-0 phase is the energetically favored state. For a larger chemical potential $-\Delta\mu < \mu < 0$, only sublattice A will be occupied with one boson per site while the other sites remain empty. This phase is therefore $1/3$ filled with an order in the form of occupied horizontal stripes. Such a $1/3$ striped density phase (SD) can also occur spontaneously in the extended Hubbard model when nearest and next-nearest interactions are included [33]. However, longer range interactions are notoriously difficult in optical lattices, so that the proposed superlattice is a convenient tool to study this phase. For positive values of $\mu > 0$, the system enters the familiar uniform Mott-1 insulator with filling factor one. Continuing this analysis for larger μ , we deduce that SD- n phases with fractional filling factor $n - 2/3$ occur for $U(n - 1) - \Delta\mu <$

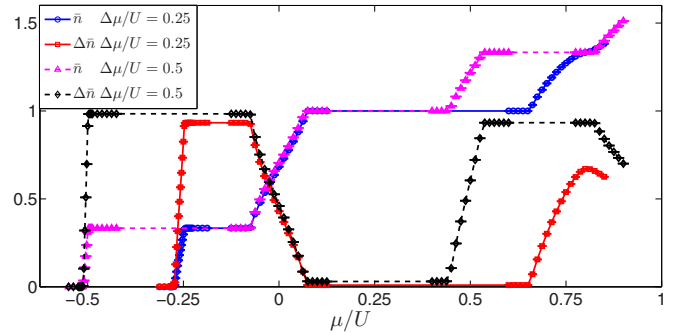


FIG. 2. (Color online) Average density $\bar{n} = (n_A + n_B + n_C)/3$ and density difference $\Delta n = n_A - (n_B + n_C)/2$ vs μ from QMC with $T = U/300$ and $N = 243$ sites at $t/U = 0.025$ for different offsets $\Delta\mu/U$.

$\mu < U(n - 1)$, which are separated by Mott- n insulators with integer filling n for $U(n - 1) < \mu < Un - \Delta\mu$.

Both the integer filled Mott- n phases and the fractional SD- n phases remain stable for small finite hopping t . As shown in Fig. 2 for $t = 0.025U$ there are plateaus of the average density $\bar{n} = (n_A + n_B + n_C)/3$ as a function of chemical potential, which are characteristic of those incompressible phases. In the fractionally filled SD- n phases the density difference $\Delta n = n_A - (n_B + n_C)/2$ between the sublattices shows plateaus with values that are slightly reduced from unity due to virtual quantum excitations. The plateau states are separated by compressible phases, which are characterized by a finite superfluid density, i.e., an off-diagonal order with a spontaneously broken $U(1)$ gauge symmetry, which will be analyzed in more detail below.

The corresponding phase diagram is mapped out in Fig. 3 using large-scale QMC simulations. The second-order GEPLT approximation is much less demanding and agrees quite well with the QMC data, except near the tips of the Mott lobes. With increasing offset $\Delta\mu$ the fractionally filled SD phases extend over a larger range not only in the chemical potential μ but also in the hopping t . In fact, the SD-1 phase for $\Delta\mu = 0.5U$ is remarkably stable up to larger values of hopping t than the uniform Mott-1 phase. The transitions to the superfluid phase are always of second order and can be understood in terms of additional condensed particles (holes) on top of the Mott states as the chemical potential is increased (decreased).

One interesting detail in the phase diagram in Fig. 3 is the drastic dependence on $\Delta\mu$ of the shape of the Mott-0 phase transition line in the limit of small hopping, which changes from linear behavior $\mu(t) = -4t$ for $\Delta\mu = 0$ to quadratic behavior $\mu(t) = -\Delta\mu - 8t^2/\Delta\mu$ for large $\Delta\mu$. The linear dependence for $\Delta\mu = 0$ can be understood from a competition of chemical potential with the kinetic energy, analogously to the quantum melting on the triangular lattice [34]. For finite $\Delta\mu$, on the other hand, the melting of the Mott-0 phase takes place by additional particles on the sublattice A only, which is not connected by any first-order hopping processes. In the limit of small t , the kinetic energy of those particles is therefore determined by the second-order hopping coefficient $\tilde{t} = t^2/\Delta\mu$, which explains the quadratic behavior of the phase boundary. The exact shape of the Mott-0 transition

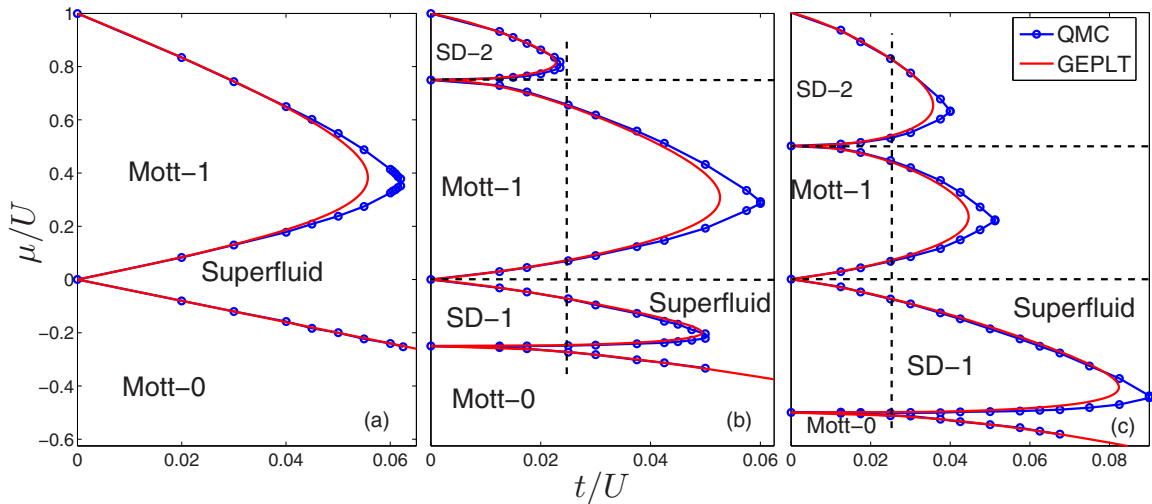


FIG. 3. (Color online) Quantum phase diagram extrapolated to the thermodynamic limit obtained from QMC (blue) and multicomponent GEPLT in second order in t/U (red) at (a) $\Delta\mu/U = 0$, (b) $\Delta\mu/U = 0.25$, and (c) $\Delta\mu/U = 0.5$. The vertical lines indicate the parameter ranges in Figs. 2 and 4 while the horizontal lines are used in Fig. 5.

$\mu = -\Delta\mu/2 - t - \sqrt{\Delta\mu^2 - 4t\Delta\mu + 36t^2}/2$ can be determined from the single-particle energy on the superlattice.

IV. ANISOTROPIC SUPERFLUID DENSITY

We now turn to the analysis of the order parameter in the superfluid phase. In the QMC simulations we determine the superfluid density along the lattice vector direction $\vec{a}_1 = (1, 0)$ using the winding number $\rho_1^s = \langle W_1^2 \rangle / 4\beta t$ and analogously for ρ_2^s along the lattice direction $\vec{a}_2 = (1, \sqrt{3})/2$ [42–44]. We use a system with $N = 243$ sites and periodic boundary conditions with $L = 9$ unit cells in both the \vec{a}_1 and \vec{a}_2 directions, which ensures that $\rho_1^s = \rho_2^s$ for the perfect kagome lattice. Note that in general the superfluid density is a response *tensor* with four elements $\rho_{xx}^s, \rho_{xy}^s, \rho_{yx}^s, \rho_{yy}^s$ in the x - y -coordinate system [45]. Due to reflection symmetry the off-diagonal elements $\rho_{xy}^s = \rho_{yx}^s = 0$ must vanish. The relation to the superfluid densities along the lattice vectors is given by $\rho_1^s = \rho_{xx}^s$ and $\rho_2^s = (\rho_{xx}^s + 3\rho_{yy}^s)/4$.

In order to analyze a possible anisotropy we consider the average superfluid density $\rho_+^s = (\rho_1^s + \rho_2^s)/2$ and the difference $\rho_-^s = \rho_1^s - \rho_2^s$ between the two lattice vector directions in Fig. 4 as a function of filling \bar{n} . For finite offsets $\Delta\mu = 0.25U$ and $\Delta\mu = 0.5U$ the superfluid density is indeed anisotropic, but surprisingly also changes the preferred direction with increasing filling \bar{n} . For low densities just above the Mott-0 phase the superfluid density is dominated by virtual hopping processes between the A sublattice. As illustrated in the left inset of Fig. 4 this virtual hopping process is not possible along the lattice vector \vec{a}_1 , which leads to an anisotropic superfluid density with $\rho_1^s < \rho_2^s$.

When the filling reaches $\bar{n} = 1/3$ the superfluid density drops to zero in the SD-1 phase as expected, but then shows the opposite anisotropy $\rho_1^s > \rho_2^s$ for $\bar{n} > 1/3$, which signals a different mechanism: At $\bar{n} = 1/3$ the A sublattice is completely filled, so that for slightly larger densities $\bar{n} > 1/3$ excess particles on the B and C sublattices are now responsible

for the superfluid density. As shown in the right inset of Fig. 4, the B and C sublattices correspond to connected chains along the \vec{a}_1 direction, which are disconnected by occupied A sites. This immediately explains why $\rho_1^s > \rho_2^s$ in this case.

According to this analysis, positive anisotropies $\rho_-^s > 0$ are therefore a hallmark of an off-diagonal U(1) order parameter coexisting with a striped density order of a filled sublattice A. This situation is reminiscent of a supersolid where a stable density order exists on one filled sublattice and excess particles contribute to the superfluidity [34], with the main difference being that in supersolids both the U(1) symmetry and the translational symmetry are *spontaneously* broken. Normally supersolid phases require longer range interactions beyond on site, which are experimentally difficult to achieve. The creation of supersolid-like regions by introducing a superlattice is experimentally straightforward, however. Similar to a supersolid, the supersolid-like regions considered here are also only stable for relatively small hopping, while for larger hopping the ordinary superfluid behavior dominates, as we will see below.

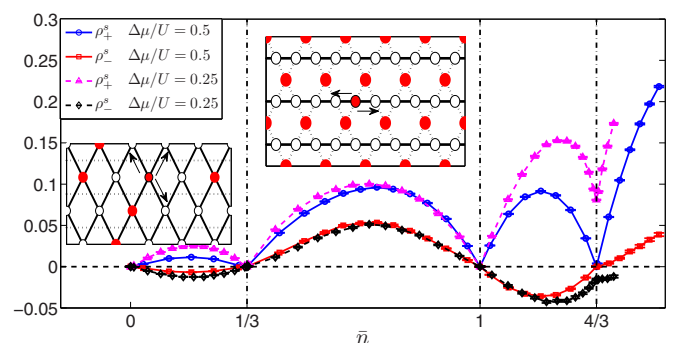


FIG. 4. (Color online) Total superfluid density $\rho_+^s = (\rho_1^s + \rho_2^s)/2$ and superfluid density difference $\rho_-^s = \rho_1^s - \rho_2^s$ vs filling \bar{n} from QMC for $\beta U = 1200$ and $N = 243$ at $t/U = 0.025$. Inset: schematic illustration of the different mechanisms for positive and negative anisotropy parameters.

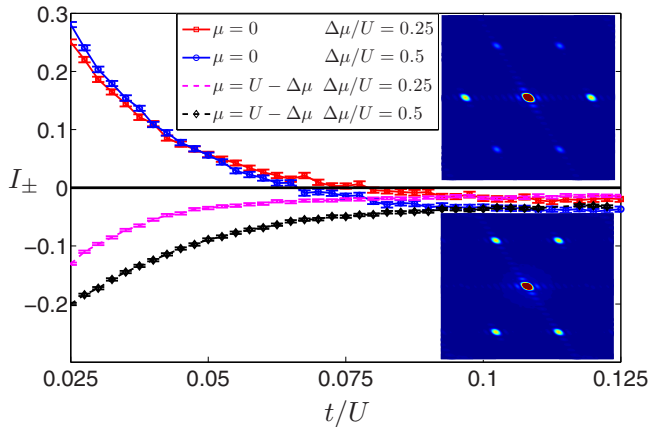


FIG. 5. (Color online) Superfluid anisotropy parameter $I_{\pm} = (\rho_1^s - \rho_2^s)/(\rho_1^s + \rho_2^s)$ as a function of t/U from QMC for $\beta U = 2000$ and $N = 432$ in the parameter range indicated by the horizontal lines in Fig. 3. Insets: QMC simulations of the TOF image for $t/U = 0.0375$, $\beta U = 800$, $N = 243$, $\Delta\mu/U = 0.5$, and $\mu/U = -0.175$ (top) and $\mu/U = 0.425$ (bottom).

As long as the hopping t/U is sufficiently small, the alternation of anisotropies between Mott and SD phases continues as the density is increased due to the same reasoning as above. However, this is not the full story, since for larger hopping t/U or larger filling \bar{n} the Mott and SD phases are not stable, so it is not clear where the different regions of positive and negative ρ_{\pm}^s are separated. Indeed, as shown in Fig. 4, the superfluid density does not drop to zero for $\bar{n} = 4/3$ and $\Delta\mu/U = 0.25$, since the corresponding line is just outside the lobe of the SD-2 phase as shown in Fig. 3(b). Also the anisotropy no longer changes sign. We find that in the limit of large hopping t/U the overall density becomes irrelevant. The sublattice A remains slightly more occupied for all values of \bar{n} and t . Since particles on the A sublattice hardly hop in the \vec{a}_1 direction, this leads to $\rho_1^s < \rho_2^s$ in the weak coupling limit $t > U$. We call this behavior the ordinary superfluid, in contrast to the supersolid-like regions of the positive anisotropy $\rho_{\pm}^s > 0$, which are basically confined between the lobes of the SD- n and Mott- n phases.

To analyze the crossover between different anisotropy regions, we show the normalized anisotropy parameter $I_{\pm} = (\rho_1^s - \rho_2^s)/(\rho_1^s + \rho_2^s)$ as a function of t/U for different values μ and $\Delta\mu$ in Fig. 5. For small hopping, the anisotropy parameter I_{\pm} is positive in supersolid-like regions ($\mu = 0$) and negative between the Mott-1 and SD-2 phase ($\mu = U - \Delta\mu$) as discussed above. For larger t/U the anisotropy parameters approach small negative values in all cases, corresponding to the ordinary superfluid. According to the analysis above, the sign change of I_{\pm} as a function of t coincides with the delocalization of the particles on the A sublattice, which starts to contribute to the superfluid density in the \vec{a}_2 direction. This behavior can be interpreted as a continuous melting of the supersolid-like phase to the ordinary superfluid, reminiscent of the melting of the sublattice order in an interaction-driven supersolid [34].

Anisotropic superfluid densities appear in a variety of different systems such as dipolar Bose-Einstein condensates

with disorder [46–49], spin-orbit coupled Fermi gases [50], coupled spin dimer systems [44], and systems with rectangular shape [51]. However, an anisotropic superfluidity which is tunable by the isotropic hopping t/U and changes sign when the order on one sublattice melts has not been discussed before, to our knowledge.

The observation of the superfluid-Mott transition by time-of-flight (TOF) experiments was pioneered many years ago [6]. The TOF absorption picture measures the momentum distribution $S(\mathbf{Q})/N = \langle |\sum_{k=1}^N a_k^+ e^{i\mathbf{Q}\cdot\mathbf{r}_k}|^2 \rangle / N^2$ and shows a clear signature of the anisotropy parameter. To demonstrate this effect, we used a QMC technique for calculating the off-diagonal long-range correlation function during the loop update [52], which allows a direct simulation of the TOF absorption signal. As shown in Fig. 5 for $\rho_{\pm}^s > 0$ (upper inset) and for $\rho_{\pm}^s < 0$ (lower inset) the TOF images display a clear signature of the anisotropy, which can be used for straightforward measurements of the melting from supersolid-like to ordinary superfluid states.

Finally, we have examined the thermal stability of the observed effects. The fractionally ordered phases are stable up to the characteristic energy scale $\Delta\mu$, but the shapes of the phase boundaries are more sensitive. In particular, to observe the parabolic shape with t near $\mu = 0$ much lower temperatures of the order $T \lesssim t^2/\Delta\mu$ are necessary. In the superfluid regions the transition temperature is approximately given by the hopping and the superfluid anisotropy turns out to be largely independent of temperature for $T \lesssim t$.

V. CONCLUSIONS

In conclusion, we analyzed ultracold bosons in a kagome superlattice, which can be created and tuned by enhancing the long wavelength laser in one direction based on recent progress for creating highly frustrated lattices [22]. By using numerical QMC simulations and the generalized effective potential Landau theory, we obtained the entire quantum phase diagram including Mott phases and fractionally filled charge density phases. In the superfluid phase an anisotropic superfluid density is found, which changes direction as the overall density, the hopping, or the interaction is varied. By tuning the hopping t/U it is possible to induce a continuous *melting* from a supersolid-like state with a filled sublattice A and positive anisotropy parameter $\rho_{\pm}^s > 0$ to an ordinary superfluid phase, which generically is characterized by a negative anisotropy parameter $\rho_{\pm}^s < 0$. Both the fractionally filled insulating phases and supersolid phases have received much attention by using models with longer range interactions [30–36]. Using the superlattice structure proposed in this work these phases become experimentally much more accessible by a simple laser setup instead of dipolar interactions. Moreover, the characteristic signature of those effects can be measured in straightforward TOF absorption experiments, without the need for single-site resolution. In particular, by implementing off-diagonal measurements in QMC loop updates, it was possible to simulate TOF flight images which show a clear signature of the anisotropic superfluid density and the change of its direction, when the melting takes place.

ACKNOWLEDGMENTS

We are thankful for discussions with D. Morath about anisotropic superfluid densities and Y. C. Wen about superlattices. This work was supported by the Allianz für

Hochleistungsrechnen Rheinland-Pfalz, by the German Research Foundation (DFG) via the Collaborative Research Center SFB/TR49, and by the Chinese Academy of Sciences via the Open Project Program of the State Key Laboratory of Theoretical Physics.

-
- [1] R. P. Feynman, *Int. J. Theor. Phys.* **21**, 467 (1982).
- [2] I. Bloch, J. Dalibard, and W. Zwerger, *Rev. Mod. Phys.* **80**, 885 (2008).
- [3] I. Bloch, J. Dalibard, and S. Nascimbène, *Nat. Phys.* **8**, 267 (2012).
- [4] M. Lewenstein, A. Sanpera, and V. Ahufinger, *Ultracold Atoms in Optical Lattices: Simulating Quantum Many-Body Systems* (Oxford University Press, Oxford, 2012).
- [5] A. Vogler, R. Labouvie, G. Barontini, S. Eggert, V. Guarrera, and H. Ott, *Phys. Rev. Lett.* **113**, 215301 (2014).
- [6] M. Greiner, O. Mandel, T. Esslinger, T. W. Hänsch, and I. Bloch, *Nature (London)* **415**, 39 (2002).
- [7] M. P. A. Fisher, P. B. Weichman, G. Grinstein, and D. S. Fisher, *Phys. Rev. B* **40**, 546 (1989).
- [8] D. Jaksch, C. Bruder, J. I. Cirac, C. W. Gardiner, and P. Zoller, *Phys. Rev. Lett.* **81**, 3108 (1998).
- [9] A. Micheli, G. K. Brennen, and P. Zoller, *Nat. Phys.* **2**, 341 (2006).
- [10] S. Peil, J. V. Porto, B. L. Tolra, J. M. Obrecht, B. E. King, M. Subbotin, S. L. Rolston, and W. D. Phillips, *Phys. Rev. A* **67**, 051603(R) (2003).
- [11] J. Sebby-Strabley, M. Anderlini, P. S. Jessen, and J. V. Porto, *Phys. Rev. A* **73**, 033605 (2006).
- [12] S. Fölling, S. Trotzky, P. Cheinet, M. Feld, R. Saers, A. Widera, T. Müller, and I. Bloch, *Nature (London)* **448**, 1029 (2007).
- [13] P. Cheinet, S. Trotzky, M. Feld, U. Schnorrberger, M. Moreno-Cardoner, S. Fölling, and I. Bloch, *Phys. Rev. Lett.* **101**, 090404 (2008).
- [14] P. Buonsante and A. Vezzani, *Phys. Rev. A* **70**, 033608 (2004).
- [15] P. Buonsante, V. Penna, and A. Vezzani, *Phys. Rev. A* **72**, 031602(R) (2005).
- [16] B.-L. Chen, S.-P. Kou, Y. Zhang, and S. Chen, *Phys. Rev. A* **81**, 053608 (2010).
- [17] A. Dhar, T. Mishra, R. V. Pai, and B. P. Das, *Phys. Rev. A* **83**, 053621 (2011).
- [18] A. Dhar, M. Singh, R. V. Pai, and B. P. Das, *Phys. Rev. A* **84**, 033631 (2011).
- [19] T. Wang, X.-F. Zhang, S. Eggert, and A. Pelster, *Phys. Rev. A* **87**, 063615 (2013).
- [20] P. Windpassinger and K. Sengstock, *Rep. Prog. Phys.* **76**, 086401 (2013).
- [21] J. Struck, C. Ölschläger, R. Le Targat, P. Soltan-Panahi, A. Eckardt, M. Lewenstein, P. Windpassinger, and K. Sengstock, *Science* **333**, 996 (2011).
- [22] G.-B. Jo, J. Guzman, C. K. Thomas, P. Hosur, A. Vishwanath, and D. M. Stamper-Kurn, *Phys. Rev. Lett.* **108**, 045305 (2012).
- [23] X.-G. Wen, *Quantum Field Theory of Many-Body Systems* (Oxford University Press, Oxford, 2004).
- [24] G. Evenbly and G. Vidal, *Phys. Rev. Lett.* **104**, 187203 (2010).
- [25] S. Yan, D. A. Huse, and S. R. White, *Science* **332**, 1173 (2011).
- [26] T.-H. Han, J. S. Helton, S. Y. Chu, D. G. Nocera, J. A. Rodriguez-Rivera, C. Broholm, and Y. S. Lee, *Nature (London)* **492**, 406 (2012).
- [27] Y. Iqbal, F. Becca, S. Sorella, and D. Poilblanc, *Phys. Rev. B* **87**, 060405(R) (2013).
- [28] S. Capponi, V. R. Chandra, A. Auerbach, and M. Weinstein, *Phys. Rev. B* **87**, 161118(R) (2013).
- [29] H. O. Jeschke, F. Salvat-Pujol, and R. Valenti, *Phys. Rev. B* **88**, 075106 (2013).
- [30] S. V. Isakov, S. Wessel, R. G. Melko, K. Sengupta, and Y. B. Kim, *Phys. Rev. Lett.* **97**, 147202 (2006).
- [31] A. O'Brien, F. Pollmann, and P. Fulde, *Phys. Rev. B* **81**, 235115 (2010).
- [32] L. F. Tocchio, C. Gros, X.-F. Zhang, and S. Eggert, *Phys. Rev. Lett.* **113**, 246405 (2014).
- [33] X.-F. Zhang and S. Eggert, *Phys. Rev. Lett.* **111**, 147201 (2013).
- [34] X.-F. Zhang, R. Dillenschneider, Y. Yu, and S. Eggert, *Phys. Rev. B* **84**, 174515 (2011).
- [35] L. Bonnes and S. Wessel, *Phys. Rev. B* **84**, 054510 (2011).
- [36] D. Yamamoto, I. Danshita, and C. A. R. Sá de Melo, *Phys. Rev. A* **85**, 021601(R) (2012).
- [37] D. Sellmann, X.-F. Zhang, and S. Eggert, *Phys. Rev. B* **91**, 081104(R) (2015).
- [38] A. W. Sandvik, *Phys. Rev. B* **59**, R14157(R) (1999).
- [39] O. F. Syljuåsen and A. W. Sandvik, *Phys. Rev. E* **66**, 046701 (2002).
- [40] K. Louis and C. Gros, *Phys. Rev. B* **70**, 100410(R) (2004).
- [41] F. E. A. dos Santos and A. Pelster, *Phys. Rev. A* **79**, 013614 (2009).
- [42] E. L. Pollock and D. M. Ceperley, *Phys. Rev. B* **36**, 8343 (1987).
- [43] A. Cuccoli, T. Roscilde, V. Tognetti, R. Vaia, and P. Verrucchi, *Phys. Rev. B* **67**, 104414 (2003).
- [44] D. Straßel, P. Kopietz, and S. Eggert, *Phys. Rev. B* **91**, 134406 (2015).
- [45] M. Ueda, *Fundamentals and New Frontiers of Bose-Einstein Condensation* (World Scientific, Singapore, 2010).
- [46] C. Krumnow and A. Pelster, *Phys. Rev. A* **84**, 021608(R) (2011).
- [47] B. Nikolic, A. Balaz, and A. Pelster, *Phys. Rev. A* **88**, 013624 (2013).
- [48] M. Ghabour and A. Pelster, *Phys. Rev. A* **90**, 063636 (2014).
- [49] A. Boudjemâa, *Phys. Rev. A* **91**, 053619 (2015).
- [50] J. P. A. Devreese, J. Tempere, and C. A. R. Sa de Melo, *Phys. Rev. Lett.* **113**, 165304 (2014).
- [51] R. G. Melko, A. W. Sandvik, and D. J. Scalapino, *Phys. Rev. B* **69**, 014509 (2004).
- [52] A. Dorneich and M. Troyer, *Phys. Rev. E* **64**, 066701 (2001).